Highlights of Spanish Astrophysics VIII, Proceedings of the XI Scientific Meeting of the Spanish Astronomical Society held on September 8–12, 2014, in Teruel, Spain. A. J. Cenarro, F. Figueras, C. Hernández-Monteagudo, J. Trujillo Bueno, and L. Valdivielso (eds.)

The life of massive stars seen through optical/infrared interferometry

Joel Sanchez-Bermudez[1], Antxon Alberdi[2], and Rainer Schödel[3]

[1] Instituto de Astrofísica de Andalucía (CSIC), Glorieta de la Astronomía S/N, 18008 Granada, Spain, e-mail: joel@iaa.es, antxon@iaa.es, rainer@iaa.es

Abstract

During the last decade, optical/infrared interferometry has become an essential tool to contribute to the understanding of stellar astrophysics. We present our results in the study of different aspects in the life of massive stars using optical interferometry. Particularly, we focused the discussion in our findings about multiplicity, interactions of the massive stars with the interstellar medium, and the early stages of high-mass stars. Our near-infrared observations comprise both: (i) long-baseline interferometry making use of AMBER/VLTI, and (ii) sparse aperture masking with VLT/NACO/SAM. These data have been obtained by our research group in the previous years, and the results have been published in several peer-reviewed papers.

The principles of the optical/near-infrared interferometry are briefly presented. Particularly, we describe how to get the calibrated Interferometric observables. Henceforth, we present our results of two massive systems (HD150136 and Herschel 36) for which we discovered their triple nature using AMBER/VLTI. Finally, we will present the recently found evidence of a disk and a binary system in a very massive young stellar object known as IRS 9A in the NGC 3603 region.

1 Introduction

Along their lives, massive stars are important actors in the enrichment and mixing of the interstellar medium. They are the principal UV-radiation sources, progenitors of the heavier chemical elements, they have strong stellar-winds, and died in the form of supernova explosions. Therefore, the evolution of galaxies cannot be fully understood without studying the formation and evolution of massive stars. Nevertheless, our understanding is still far from complete. This is because observations of massive stars are challenging due to their rareness, location at large distances from the solar system($\geq$1 kpc), high-extinction, and their short lifetimes ($\sim$Ma) [27, 5].

There are two contemporary models that aim to explain high-mass star formation: (i) core collapse (or monolithic collapse) and, (ii) competitive accretion. The main difference between both of them is the way in which massive stars gather mass during their formation process. **Core collapse** suggests that the total mass of forming high-mass is determined since the beginning of the collapsing phase. Therefore, the mass of the forming star is constrained only by the total mass of the massive molecular core from which they are formed [14, 9]. In contrast, **competitive accretion** is based on the inefficiency of the cloud fragmentation. This model predicts that massive stars are initially formed from pre-stellar cores with masses around the Jeans mass (0.5 $M_{\odot}$) and subsequently accrete material from their environment. In competitive accretion, the total reservoir of gas available in the cloud affects the massive star formation process. The pre-stellar cores located at the center of the gravitational potential tend to accrete more material, forming massive stars. On the other hand, pre-stellar cores located in low-density regions in the cloud form low-mass stars. This model does not only predict a mechanism to form massive stars, but a complete initial mass function (IMF) for an entire cluster [3, 2].

There are important observational differences predicted by the aforementioned models. Both of them invoke accretion during the star formation process via accretion disks [1, 10]; however, core collapse suggests the presence of large accretion disks with sizes around ∼1000 AU, while competitive accretion predicts smaller disks (∼100 AU) truncated by possible encounters with other stellar objects. Another intriguing characteristic is the role of multiplicity in the massive stars formation process. The current observational studies over a sample of more than 100 O-type stars in the southern hemisphere suggest that $\sim$ 90% of the sources have at least one stellar companion. In fact, around one quarter of the sample belong to a high-degree multiple system [19]. Both massive star formation models invoke the possible formation of stellar companions due to inhomogeneities in the accretion disks. However, the number of components in multiple systems do not exclude stellar capture, due to encounters with other systems, as an additional mechanism of formation. In this context, testing the coplanarity of the orbits could provide important hints of the early dynamics and formation of massive multiple systems.

During the last decade, our understanding of multiplicity of massive stars and their early stages has been improved, particularly thanks to the advent of Adaptive Optics (AO; $\theta_{max} \sim 100$ mas) in 8-meter telescopes, the start up of long-baseline interferometric facilities like the Very Large Telescope Interferometer (VLTI; $\theta_{max} \sim 2$ mas), and the implementation of techniques like Sparse Aperture Masking (SAM; $\theta_{max} \sim 35$ mas). In this brief review, we describe our studies of (i) the multiplicity, (ii) the interactions of windy massive stars with the interstellar medium, and (iii) the early stages of massive stars making use of the European Southern Observatory (ESO) interferometric facilities.

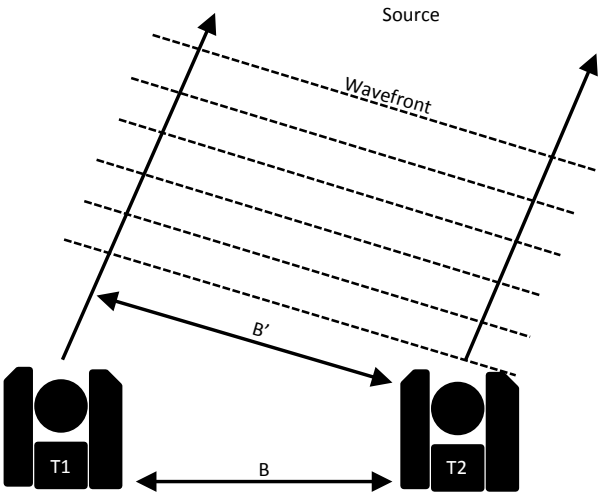

Figure 1: Schematic of a simple interferometer composed of two telescopes (T_1 and T_2). The resolution of the interferometer is $\Theta = \lambda/B'$, where B' is the projected baseline between the two telescopes in the plane of the sky, and λ the wavelength of the observations. The incoming wavefronts are represented in the diagram with the dashed lines.

2 Highlights of optical interferometry

2.1 Differences between optical and radio interferometry

Interferometry is nowadays a crucial tool for modern astrophysics. It has permitted to increase the resolution of astronomical observations from $\Theta = \lambda/D$, where D is the telescope diameter, to $\Theta = \lambda/B$, where B is the projected separation between telescopes or antennas (See Fig 1). The first experiments to obtain information of the brightness distribution of astronomical objects from interferometric fringes were performed at optical wavelengths more than one century ago. For example, one could refer the work of Michelson in 1891 to measure the diameters of the four major satellites of Jupiter, using a couple of variable spacing slits to mask a 12-inch aperture telescope [12]. However, it was not until 1967 when the the coherent light of two separated telescopes were successfully combined by Labeyrie [11]. Nevertheless, the restrictions imposed by the turbulent atmosphere and the technological limitations to perform interferometric observations at $\lambda \leq$100 μm, relegate the development of this technique until the 90s. In contrast, the large *coherence time* and *coherence lenght* of radio wavelengths ($\lambda \sim$ cm), and the high transparency of the atmosphere at these wavelengths, allowed to use and develop radio interferometry since the late 40s becoming a widely-used technique from the 80s.

Although interferometry itself uses the phenomena of the interference of light and it is, in principle, independent of the wavelength, there are several differences between optical/infrared and radio interferometry that goes from (i) the role of the atmosphere, (ii) the

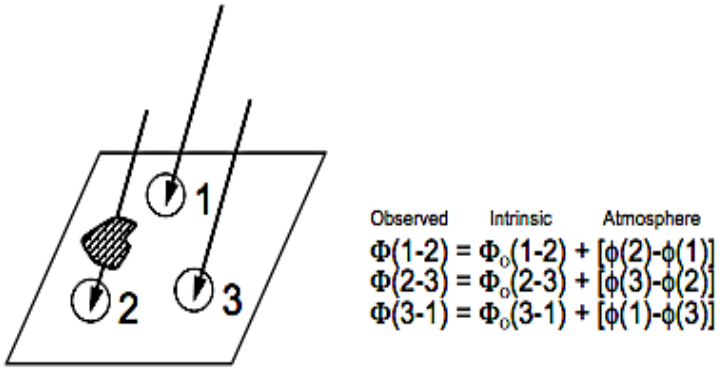

Figure 2: Schematic of closure phase construction. A closure phase is constructed multiplying the **observed** phase information of tree telescopes (black circles), which baselines form a closed triangle. This product eliminate the errors induced in the **intrinsic** phases (which contain information that depends only on the brightness distribution of the source) due to the effect of the **atmosphere**.

spatial and temporal scales of the received wavefronts, and (iii) technological restrictions. Therefore, there are important distinctions in the form in which the interferometric data are acquired and reduced between both regimes.

In the case of radio interferometry, the sampled signal is collected via radio antennas, which transform the received electric field into a electrical signal amplified at the focus of the antennas. The coherent interference of the measured electric potentials at each antenna is performed subsequently via a digital *correlator*. On the other hand, optical/infrared interferometry uses optical elements (i.e. glasses and mirrors) to collect and interfere the light of the target. The difference in the correlation of the data between both techniques has an impact in the spectral information that can be recorded, while radio interferometers have spectral resolutions R$\sim 10^5$, optical interferometers have only reached moderate spectral resolutions R$\sim 10^3$.

The observables are also different between both techniques. The basic theory of interferometry is described with the van-Cittert Zernike Theorem [25]. This theorem describes the *visibility function*, $V(u, v)$, which is the main observable in interferometry. $V(u, v)$ describes the Fourier transform of the projected brightness distribution of the target convolved with the transfer function of the interferometer (or a synthesized beam). In radio astronomy, the observables are directly the amplitude (V) and phase (Φ) of the visibility function. However, in optical/infrared interferometry, the turbulence of the atmosphere corrupts the phase information. Therefore, the *closure phase* (CP) is used. This observable eliminates the telescope-dependent phase noise and provides phase information that only depends on the

structure of the source. Fig. 2 displays a diagram of the construction of the closure phases. Moreover, in contrast to radio astronomy, in optical interferometry instead of working with the amplitude of the visibilities, the observable is the squared visibility. This provides a better representation of the total power encoded in the interferometric fringes.

Similar to radio interferometry, the observables of optical interferometry should be calibrated to account for the transfer function (or point spread function) of the instrument. Calibrators are point-like sources that should be observed with similar conditions as the targets of interest. Therefore, calibrators should not be located more than 2° from the target. Consequently, interwoven observations between calibrator and target are scheduled for observations. Fig 3 displays, as an example, the calibrated V^2 and CPs for IRS 1W, one of the massive stars located at the central parsec of the Galactic center (GC) studied by our group [23].

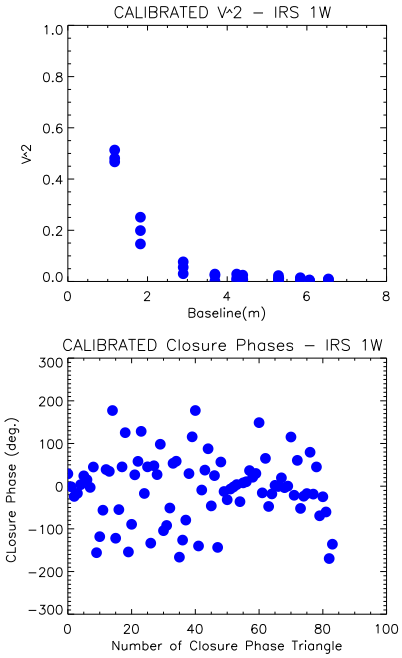

Figure 3: Calibrated V^2 and CPs. The data were taken with NACO/VLT at 3.8μm. Notice that the source IRS 1W is resolved and clearly asymmetric, since the closure phases exhibit strong variations between -180° and 180°.

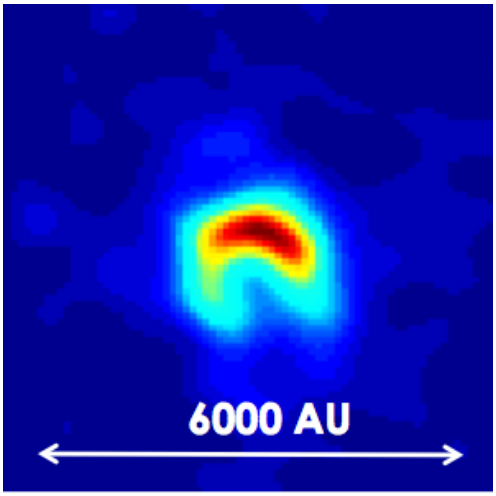

Figure 4: Reconstructed BSMEM image of IRS 1W. The source exhibits an asymmetric morphology similar to a horseshoe. The observed structure corresponds to the bowshock generated by the strong wind of the central star (not observed at this frequency) and the interstellar medium in which the source is moving.

Once the interferometric observables are calibrated, it is possible to reconstruct the intrinsic brightness distribution of the source via a Fourier transform (FT), even in the case of relatively poor u-v coverage. However, the FT image have contrast that need to be eliminated. In radio interferometry, the most common used method is the CLEAN algorithm [7]. In optical interferometry, it is more suitable to use algorithms like the *Maximum Entropy Method (MEM)*. MEM performs image reconstruction by fulfilling two criteria: i) the model of the reconstructed image should fit the interferometric observables; ii) the best image

should also maximizes the *entropy* [6, 24, 17]. One of the best software to perform image reconstruction in optical interferometry is BSMEM [4], which perform a direct model fitting to the V^2 and CPs. Fig. 4 displays the reconstructed image using BSMEM for the data set presented previously for IRS 1W. It is a research field under development. In fact, to test the different algorithms, methodologies and software to perform image reconstruction, the community of optical interferometry perform a biennial competition, known as the "Beauty Contest" [13]. In the 2014 edition, our group was the winner [16]. For a more detailed review on optical interferometry see [15].

2.2 Sparse Aperture Masking

An imaging technique that has gained importance during the last years is sparse aperture masking (SAM). This method transforms a single dish telescope into a Fizeau interferometer by placing a mask with several holes at the pupil plane of the detector. The holes in the mask act as small telescopes that form a non-redundant interferometric array. The observed data at the detector consisted in a superposition of the different fringes generated by the interferometric array, known as *interferogram*. This technique provides a very-well defined PSF. The low uncertainties of the closure phases allows the reliable reconstruction of the images up to a resolution $\Theta = \lambda/2B_{max}$. Another advantage of this technique is that it provides very high signal to noise ratio (SNR), typically on the order of SNR$\sim$100-500. This is very useful for the detection of faint stellar companions or planetary bodies, particularly at angular scales where other techniques like coronagraphy does not work. In contrast, since most of the pupil area is covered with the non-redundant mask, this technique is limited to be used with bright sources. For example, the range of magnitudes covered with the infrared camera NACO/VLT goes from $6 \leq \text{mag} \leq 12$. Fig. 5 shows the interferogram observed at the NACO/VLT detector for IRS 7 (a super giant star at the inner parsec of the GC), its Fourier transform, and the u-v coverage of the observations.

3 Massive stars at their early stages: The case of NGC 3603 IRS 9A*

Observations of the early phases in massive stars are challenging, particularly because young high-mass stars are highly extinguished by the large amount of gas and dust of their parental clouds. The current massive star formation theories suggest the presence of disk-like structures at the core of massive young stellar objects (MYSOs). However, these structures have been elusive for some of the most massive young stars. Therefore, the study of individual objects, where such disks may be observed, is of astrophysical importance. Here, we presented the study of the young stellar object NGC 3603 IRS9A* with NACO/SAM observations and CRIRES/VLT spectroastrometric data. The NACO/SAM data were taken at two filters in the near-infrared: Ks (2.2 μm) and L' (3.8 μm). The CRIRES data correspond to the H_2 (2.121 μm) and $Br\gamma$ (2.166 μm) lines. These lines were observed with a long-slit located at three different angles 0°, 90° and 128°, with a resolving power of about R$\sim$33000.

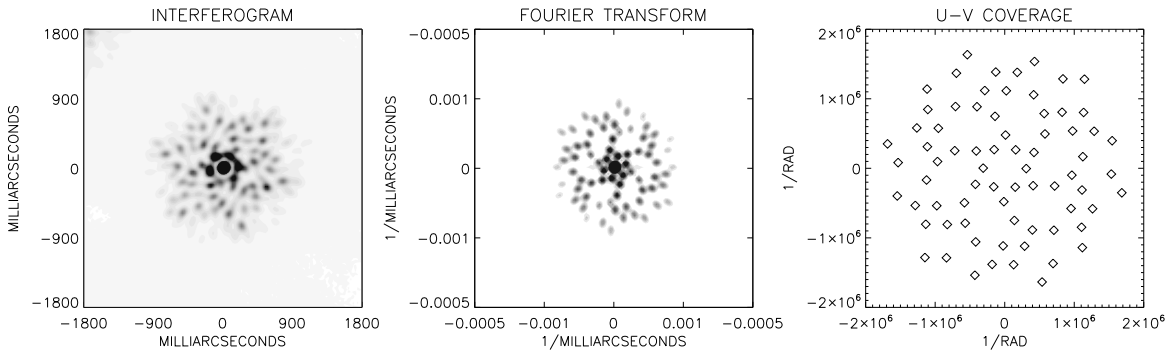

Figure 5: **Left:** The interference pattern of IRS 7 observed at the NACO/VLT detector, using a non-redundant mask with 9 holes. The data correspond to observations in the L' filter. **Center:** The Fourier transform of the sampled interferogram. This is also known as the auto-correlation function. **Right:** The spatial frequencies covered with the used mask.

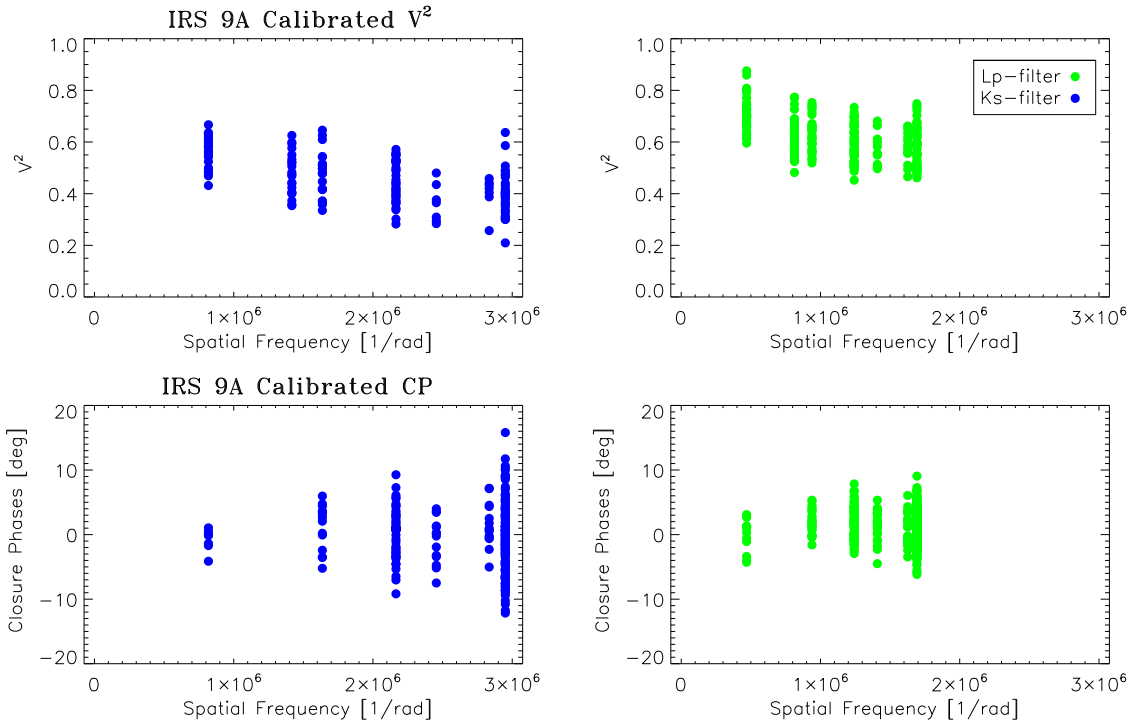

Figure 6: Calibrated V^2 and CPs of the NACO/SAM observations taken at K_s and L' filters. Notice how the observables support the existence of a partially resolved target at both frequencies. The vertical variation of the V^2 per baseline is caused due to the seeing variations at the time of the observations. In contrast, closure phases are free of telescope phase errors, and depends only to the structure of the target.

The new SAM data were reduced following the standard procedure for this kind of data (see Sec. 2.2). The interferometric observables for both filters display a partially resolved target with an additional over-resolved component. Fig 6 displays the observed V^2 and CPs of IRS 9A. Notice how the V^2 decrease from the shortest to the largest baselines, while the CPs have small variations between -10° and 10°. The best-fit geometrical model, consisting of a uniform disk, determined an angular size of around ∼30 milliarcseconds (mas) for the compact component, with a correlated flux at zero baseline that goes from V^2 ∼50 to 70 % of the total flux. This implies the presence of an extended component with an angular size ≥200 mas. These findings agree with previous observations of NGC 3603 IRS 9A* at mid-infrared wavelengths with T-ReCS at the Gemini Telescopes and with MIDI/VLTI [26], which identified also two components associated to an inner warm-disk plus a cold envelope. Similar findings were derived from the spectroastrometric analysis of the lines observed with CRIRES. Tracking the centroid of the flux at the H_2 emission line suggest that this line arises from angular scales between 150 to 300 mas, depending on the angle of observation. On the other hand, Brγ appears to be formed at the very center of the target, at regions more compact than ≤ 20 mas.

It is important to highlight that, although the Brγ appears to be formed at the same angular scales of the proposed warm-disk, the behavior of the spectroastrometric signal does not correspond to a simple rotating disk in Keplerian rotation. In contrast, the observed sprectroastrometric signal suggests the existence of a more complex morphology at the core of IRS 9A. To perform a more complete description of the physics of the target, we proposed a complete radiative transfer model that fit simultaneously the observed V^2 for the near-/mid-infrared wavelengths and the spectral energy distribution. Fig 7 displays the best-fit radiative transfer model of the observed V^2 with the different instruments. It is observed that the model is consistent at all the observed wavelengths. However, it still presents some deviations, particularly at the shortest baselines of the T-ReCS data. Nevertheless, this is not unexpected since these baselines corresponds to angular scales ≥1" (or 7000 AU at 7kpc), and the environment around IRS 9A presents some additional components at scales between 1"-2", that can contribute to the observed flux at mid-infrared wavelengths (see Fig 4 of [18]). For a more complete description of the scientific analysis, that we performed on this target see [21]

4 Multiplicity in massive stars: HD 150136 and Herschel36

Another intriguing property of massive stars is multiplicity. A high percentage of the observed massive stars belong to a binary or higher-degree multiple system. There is a still open debate about the mechanisms to form these high-mass multiple systems. The most accepted ones invoke the formation of close companions by irregularities in the accretion disks around MYSOs. However, there is not a consensus on the formation of triple and higher-degree multiple systems. Are those systems common in massive stars? Are massive multiple systems stables, or do they tend to break apart forming isolated targets (e.g., run-away stars)? How does the distribution of masses, eccentricities, and brightness ratios change depending on the spatial scales at which companions are formed? These are some of the open questions

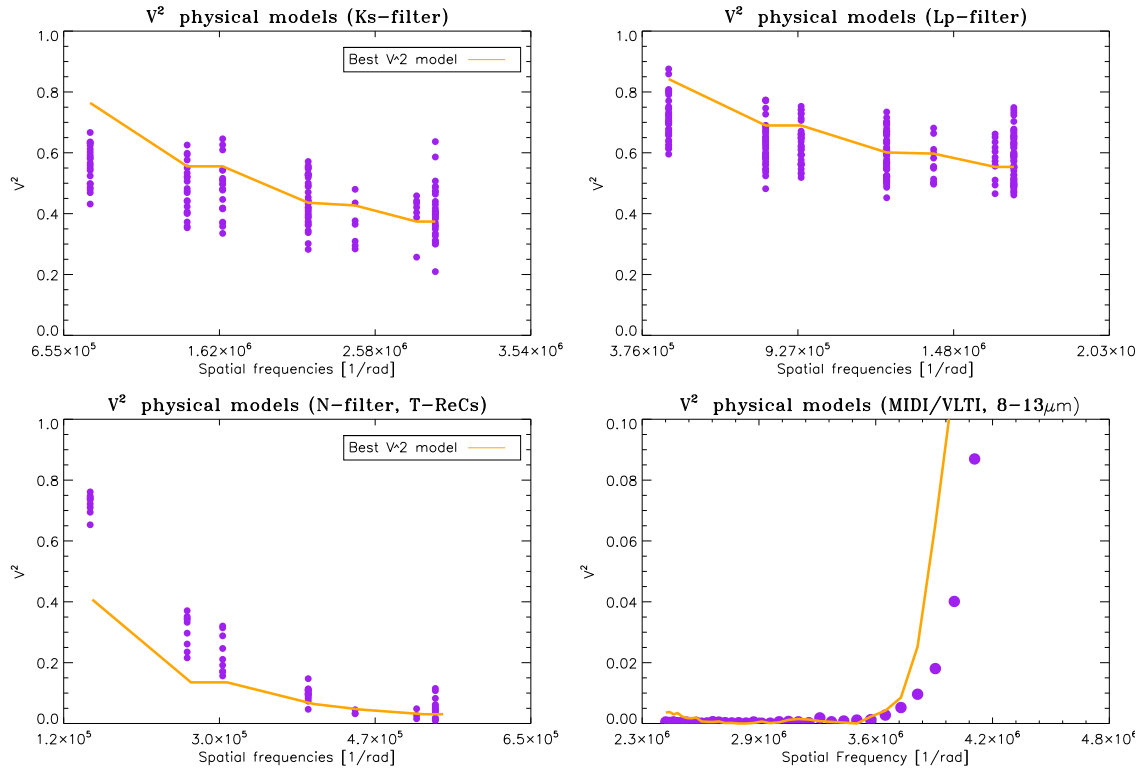

Figure 7: Best-fit physical model applied to the interferometric data of IRS 9A. The different data sets are displayed in purple filled dots and the model in orange lines. The physical model consisted in a warm disk of 20 mas surrounded with a cold envelope of 2" that has polar cavities with an opening angle of 30°.

that are yet under scrutiny. Following this scenario, coplanarity among orbits in massive multiple systems could allow us to infer the early dynamics of the systems and determine their formation mechanisms.

In the last years, our group has studied two peculiar triple hierarchical systems targets: HD 150136 and Herschel 36. On the one hand, **HD150136**, at a distance of 1.3 kpc, is the nearest massive system to the Earth with a total mass of above 100 $M_{\odot}$ and an O3 star as a primary. Thus, this system represents a unique candidate to study multiplicity at the upper end of the initial mass function (IMF). On the other hand, **Herschel36**, is responsible for most of the gas ionization in the M8 nebula (1.3 kpc). Due to its multiplicity and role this system has been compared with Θ^1 Ori C [8]. Both systems consist of an spectroscopic binary with a period of ∼days, and a separated additional component with a much larger period (P∼years). This last one can be imaged with optical interferometry.

We made use of the AMBER/VLTI instrument, with a maximum angular resolution of 2 mas, in its low-resolution mode (LHK; R=36). The main goals of our research were to (i) confirm the triple nature of the systems, (ii) determine the contrast ratio between the tertiary component and the spectroscopic binaries, (iii) determine their position angles, and (iv) provide a first order approximation of their orbits. Since the separation between components for the spectroscopic binaries were well beyond the angular resolution of AMBER, only the

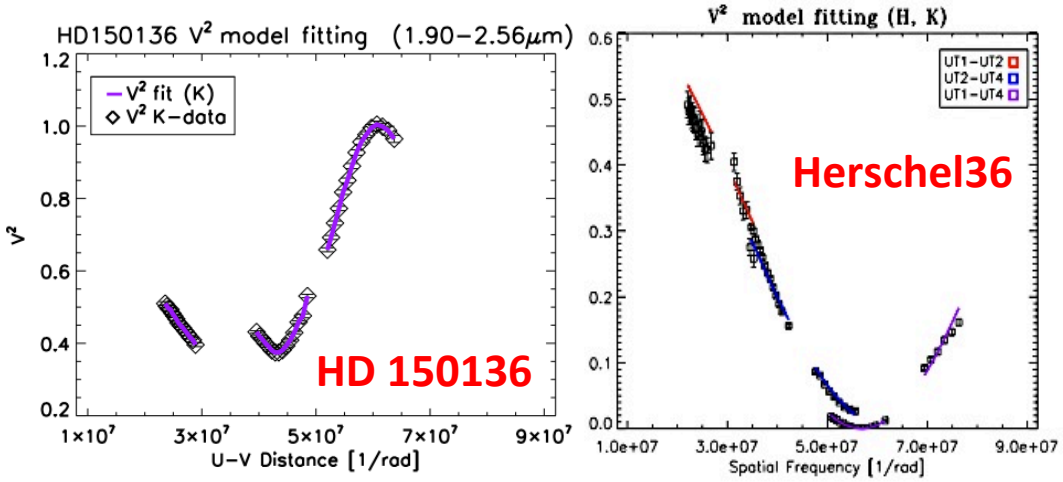

Figure 8: Calibrated V^2 of HD 150136 and Herschel36. The data are displayed in black diamonds and squares. The best-fit geometrical model are displayed as continuous lines of different colors.

component located farther away was resolved. Fig 8 displays an example of the calibrated V^2. Notice how the signature of the observables clearly traces a cosine function, typical of a binary target (spectroscopic binary+tertiary). Similar trend is observed in the CPs.

Table 1: Best-fit geometrical models applied to HD 150136 and Herschel36

Parameter	HD 150136	Herschel36
$f_{overresolved}$ [a]	-	0.17
f_{inner} [b]	0.80	0.41
f_{outer} [c]	0.20	0.42
$d[mas]$ [d]	7.27	1.81
$\Phi[deg]$ [e]	209.0°	222.0°

[a] Fraction of total over-resolved flux.
[b] Fraction of total flux contained in the spectroscopic binary.
[c] Fraction of total flux contained in the outer component.
[d] Angular separation between the hard binary and the outer component in milliarcseconds.
[e] Position angle between components projected in the plane of the sky and measured to the east of north.

Geometrical models of a binary source, with unresolved point-like objects, provided the orientation and contrast ratio of the components in the systems. Table 1 displays the best-fit parameters obtained. Moreover, our interferometric data, in combination with spectroscopic observations, allowed us to provide a first estimate of the orbits. In the case of HD 150136 there were two additional optical interferometry epochs observed with PIONIER/VLTI, which in combination with our AMBER/VLTI data, constrained the period of the outer orbit to 2770 days. In contrast, for Herschel36, there was only one astrometric epoch; hence, we could

barely constrain the parameters for the orbit of the system. Future work includes a follow-up of the orbits for both systems, to determine whether they are coplanar or not. This is a clear indication of the formation scenario. For more information about these studies see [22, 20]

5 Summary

Optical interferometry has consolidated itself during the last decade as one of the most important high-angular resolution techniques in modern Astronomy. Although the basis of the technique is the same as in radio interferometry, the technical implementation and the nature of the light at infrared wavelengths imply important changes in the measured interferometric observables, and their data reduction. During the last four years, our group has performed several studies using optical interferometry (in its different categories) to perform studies of several aspects of massive stars. In NGC 3603 IRS 9A*, optical interferometry has allowed us to determine a complete picture of its morphology along different angular scales that go from 0.025"-1". Moreover, these studies enhance the importance of the use of optical interferometry to constrain more suitable models that describe the morphology of the target, in contrast with models that only use information from the SED, which tend to be degenerated. From our work with the triple hierarchical systems, we determined its triple nature without ambiguity, mapping for the first time their components. This was just the first step to a more detailed analysis of the dynamics of these systems, which will provide important clues on their formation and evolution.

These discoveries represent only one of the branches in which optical interferometry is useful. There are other fields of research including planetary nebulae, AGNs, or evolved stars. The experimental situation will improve in the next years, thanks to the first light of the second generation of instruments (MATISSE and GRAVITY) at the VLTI, improving the current sensitivity by $\sim$5 mag, and allowing higher quality image reconstruction. Hence, this update will open a huge range of new targets that could be studied with this techniques.

Acknowledgments

J.S.B., R.S. and A.A acknowledge support by grants AYA2010-17631 and AYA2012-38491-CO2-02 of the Spanish Ministry of Economy and Competitiveness (MINECO) cofounded with FEDER funds, and by grant P08-TIC-4075 of the Junta de Andalucía. R.S. acknowledges support by the Ramón y Cajal program of the Spanish Ministry of Economy and Competitiveness. J.S.B. acknowledges support by the "JAE-PreDoc" program of the Spanish Consejo Superior de Investigaciones Científicas (CSIC), and to the support of the Sociedad Española de Astronomía for its support to participate in its XI scientific meeting in Teruel, Spain.

References

[1] Bonnell, I. A., & Bate, M. R., 2002, MNRAS, 336, 659-669

[2] Bonnell, I. A., & Bate, M. R., 2006, MNRAS, 370, 488-494

[3] Bonnell, I. A., Vine, S. G., Bate, M. R., 2004, MNRAS, 349, 735-741

[4] Buscher, D. F., 1994, Very High Angular Resolution Imaging; eds. Robertson, J. G., & Tango, W. J., 158, 91

[5] Evans, II, N. J., 1999, ARA&A, 37, 311

[6] Gull, S. F., & Skilling, J., 1983, Measurement and Processing for Indirect Imaging, eds. J.A. Roberts; Cambridge University Press, 267

[7] Högbom, J. A., 1974, A&A, 278, 328

[8] Kraus, S., Hofmann, K.-H., Malbet, F., et al., 2009, A&A, 787

[9] Krumholz, M. R., 2006, ApJ, 641, L45-L48

[10] Krumholz, M. R., Klein, R. I., McKee, C. F., Offner, S. S. R., & Cunningham, A. J., 2009, Science, 323, 754

[11] Labeyrie, A., 1975, ApJ, 196, L71

[12] Labeyrie, A., Lipson, S. G., & Nisenson, P., 2006, An introduction to Optical Stellar Interferometry, Cambridge University Press

[13] Lawson, P. R., Cotton, W. D., Humel, C. A., et al., 2004, SPIE Conference Series: New Frontiers in Stellar Interferometry, 886, doi:10.1117/12.550710

[14] McKee, C. F., & Tan, J. C., 2002, Nature, 416, 59-61

[15] Monnier, J. D., Allen, R. J., 2012, Planets, Stars & Stellar Systems, Springer,

[16] Monnier, J. D., Berger J. P., Le Bouquin, J. B., 2014, SPIE Conference Series: Optical and Infrared Interferometry VI, 9146, doi: 10.1117/12.2057312

[17] Narayan, R., & Nityananda, R., 1986, ARA&A, 24, 127

[18] Nürnberger, D. E. A. 2008, Journal of Physics Conference Series, 131, 012025

[19] Sana, H., Le Bouquin, J.-B., Lacour, S., et al., 2014, ApJS, 215, 15

[20] Sanchez-Bermudez, J., Alberdi, A., Schödel, R., et al., 2014b, A&A, 572, L1

[21] Sanchez-Bermudez, J., Hummel, C. A., Tuthill, P., et al., 2014c, arXiv:1409.2831

[22] Sanchez-Bermudez, J., Schödel, R., Alberdi, A., et al., 2013, A&A, 554, L4

[23] Sanchez-Bermudez, J., Schödel, R., Alberdi, A., et al., 2014a, A&A, 567, A21

[24] Skilling, J., & Bryan, R. K., 1984, MNRAS, 211, 111

[25] Thompson, A R., Moran, J. M., & Swenson Jr., G. W., 2001, Interferometry and Synthesis in Radio Astronomy, 2nd Edition, Wiley

[26] Vehoff, S., Hummel, C. A., Monnier, J. D., et al., 2010, A&A, 520, A78

[27] Zinnecker, H., & Yorke, H. W., 2007, ARA&A, 45, 481-563